Supplementary Material

Aβ Plaque-Selective NIR Fluorescence Probe to Differentiate Alzheimer's Disease from Tauopathies

K. Rajasekhar,[1] Nagarjun Narayanaswamy,[1] N. Arul Murugan,[2] Keith Viccaro,[3] Hyoung-Gon Lee,[4], Kavita Shah,[3] Thimmaiah Govindaraju[1]*

[1] Bioorganic Chemistry Laboratory, New Chemistry Unit, Jawaharlal Nehru Centre for Advanced Scientific Research, Jakkur P.O., Bengaluru 560064, Karnataka, India

[2] Division of Theoretical Chemistry and Biology, School of Biotechnology, KTH Royal Institute of Technology, S-106 91 Stockholm, Sweden

[3] Department of Chemistry and Purdue University Center for Cancer Research, 560 Oval Drive, West Lafayette, IN 47907, USA.

[4] Department of Biology, The University of Texas at San Antonio, One UTSA Circle, San Antonio, TX 78249, USA

Table of Contents

I. Experimental details

1.1 Synthesis of probe CQ

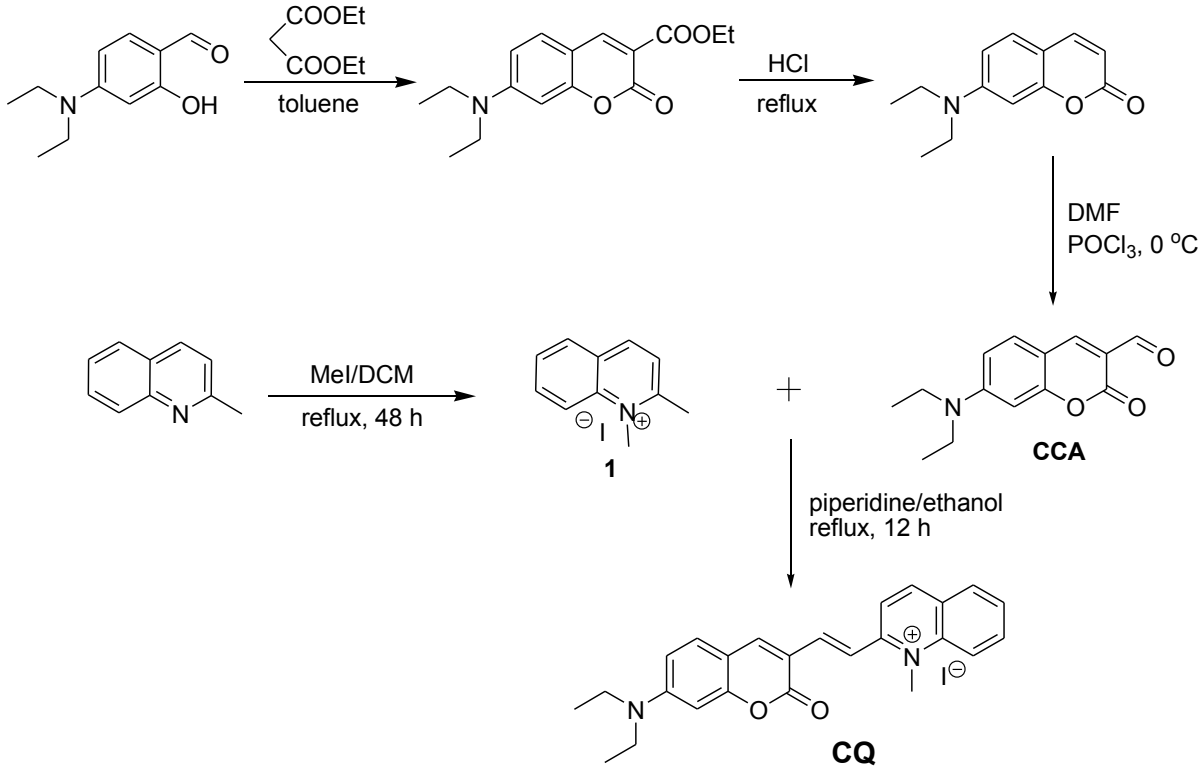

Synthesis of 1,2-dimethylquinolin-1-ium iodide (1) and 7-(diethylamino)-2-oxo-2H-chromene-3-carbaldehyde (CCA)

2-Methylquinoline (1 mL, 7 mmol) and iodomethane (2 mL, 28 mmol) were stirred under nitrogen atmosphere in DCM (10 mL) at 55 °C for 48 h. The completion of reaction was monitored with TLC. After completion of the reaction, the solvent was evaporated under vacuum. Yellow-colored crude product was obtained, which was used in subsequent reaction without any further purification. 7-(Diethylamino)-2-oxo-2H-chromene-3-carbaldehyde (CCA) was synthesized by following the reported procedure from our group (Scheme) (Maity et al., 2010).

Synthesis of 2-(2-(7-(diethylamino)-2-oxo-2H-chromen-3-yl)vinyl)-1-methylquinolin-1-ium iodide (CQ)

To a stirred solution of compound **1** (40 mg, 0.14 mmol) in ethanol (2 mL), piperidine (5 μL) was added. After 10 min., 7-(diethylamino)-2-oxo-2H-chromene-3-carbaldehyde (CCA) (20 mg, 0.08 mmol) in DCM (2 mL) was added to above reaction mixture. The reaction mixture was stirred at reflux condition under nitrogen atmosphere for 3 h. After completion of the reaction, solvent was evaporated and the crude product was purified using column chromatography on silica gel using chloroform: methanol (95:5) solvent system to obtain **CQ** in good yields (70%).

^{1}H NMR (*DMSO* d_6, 400 MHz) δ 8.98-8.96 (d, J = 8 Hz, 1H), 8.50-8.30 (m, 3H), 8.176-8.172 (d, J = 1.6 Hz, 1H), 8.15-8.13 (m, 3H), 8.13 (s, 1H), 8.10-7.91 (m, 1H), 7.89-7.58 (m, 1H), 6.86-6.65 (m, 1H), 6.64 (s, 1H), 4.46 (s, 3H), 1.18-1.49 (m, 6H); ^{13}C NMR (*DMSO* d_6, 100 MHz) δ159.7, 156.7, 156.2, 152.6, 147.1, 143.4, 142.7, 139., 134.7, 131.3, 130, 127.4, 120.5, 119, 117.6, 113, 110.4, 108.5, 96.3, 44.4, 12.3; HRMS (ESI-MS): found 385.1916, calcd. for $C_{25}H_{25}IN_2O_2$ $[M-I]^+$ m/z = 385.1911.

1.2 Preparation of IAPP fibrillar aggregates. A 0.1 mg (Merck, calbiochem) sample of IAPP was dissolved in 100 μL of acetonitrile to disrupt any pre-existing aggregates, and taken up in 200 μL by adding 10 mM PBS buffer (pH 7.4). The final concentration of acetonitrile in the fibrillization buffer was 10% (v/v). Then the solution was sonicated continuously for 1 min to break up any potential aggregates. To form fibrils, the sample was incubated at 37 °C without agitation in an eppendorf tube for 120 h (5 days). The formation of IAPP fibrillar aggregates was confirmed by ThT assay.

1.3 Preparation of α-Syn fibrillar aggregates. α-Synuclein (α-Syn) peptide (0.5 mg) (Sigma Aldrich) was dissolved in hexafluoro-2-propanol (HFIP, 0.2 mL) and incubated at room temperature for 1 h. HFIP was then removed by a flow of nitrogen and further dried under vacuum and re-dissolved in TBS buffer to a concentration of 200 μM. Then the solution is incubated at 37 °C for 3-5 days with constant shaking of 150 rpm.

1.4 Preparation of Tau fibrillar aggregates. tau protein was dissolved in PBS buffer (10 mM, pH 7.4) to a concentration of 100 μM. Then the tau protein is diluted into aggregation buffer [PBS, dithiothreitol (1 mM)] to the desired concentration (10 μM) and incubated for 3 h at 37 °C. Then the aggregation is initiated by the addition of heparin (50 μM) to the sample and incubated for 72 h at 37 °C to obtain fibrillar aggregates.

1.5 Calculation of partition coefficient (log P). Log P value was calculated by Shake flask (or tube) method. To an equilibrated solution of n-octanol and water in a separating funnel probe **CQ** was added and agitated. The solution was left for 30 min for proper separation of immiscible solvents, then the distribution of **CQ** was calculated using UV spectroscopy and the obtained concentrations were used in below equation to obtain log P value.

log P = log [Conc. of **CQ** in n-octanol/Conc. of **CQ** in water]

1.6 Quantum yields determination. Emission spectra of **CQ** with and without Aβ42 fibrillar aggregates were recorded. Cresyl violet perchlorate in ethanol (ϕ = 0.54) was used as the standard for the fluorescence quantum yield calculation using the absorption of the test sample. The emission spectra area was obtained from 550-800 nm. Dilute solutions (10^{-6} M) were used to minimize reabsorption effects. Fluorescence measurement were made three times for each dye and averaged. Quantum yields were determined using the following equation

$$\phi_{CQ} = \phi_{stand} (F_{CQ}/F_{stand}) \times (A_{stand}/A_{CQ}) \times (n_{CQ}^2/n_{stand}^2)$$

ϕ = Quantum yield, **F** = Area under fluorescence spectra, **A** = Absorbance, **n** = Refractive index

1.7 *In vitro* stability study of probe CQ in human serum. The *in vitro* stability of **CQ** in human serum was determined by incubating **CQ** (10 μM in H_2O, 50 μM) with 300 μL of human blood serum at 37 °C for 30 and 60 min. All the serum proteins were precipitated by adding 500 μL of acetonitrle after centrifugation at 5000 rpm for 5 min at 4 °C. The supernatant was collected. Approximately 0.1 mL of the supernatant solution was analyzed using liquid chromatography mass spectroscopy (LCMS) (Fig. S8).

1.8 Cell viability assay. To assess the cytotoxicity of probe **CQ**, MTT assay was performed. PC12 cells were seeded in a 96-well plate at a density of 12,000 cells/well in RPMI medium (Gibco, Invitrogen) with foetal bovine serum (FBS, 10%), horse serum (HS, 5%) and pen strep (1 %) at 37 °C in an atmosphere of 5 % CO_2 for 24 h. Then the cells were treated with increasing concentrations of probe **CQ** and incubated for 24 h at 37 °C in an atmosphere of 5 % CO_2. Then 10 μL of MTT (5 mg/mL solution in PBS) was added to each well and incubated for 3 h. Subsequently, the media was discarded and 100 μL of 1:1 (DMSO: methanol) solution was added, the reduced MTT was measured by recording absorption at 570 nm and 690 nm (background).

1.9 Molecular dynamics and free energy simulations. In order to understand the ThT displacement by **CQ** probe we carried out combined molecular dynamics and MM-GBSA based free energy calculations for each of **CQ**+amyloid fibril complexes (Frisch et al., 2010; Lührs et al., 2005; Lesne et al., 2006; Morris et al., 2009; Miller et al., 2012). As we described in the results and discussion section, there are four different binding sites (the most

populated) for **CQ** probe in amyloid fibril. For each of these complexes, MD and binding free energy calculations were performed. The fibril:**CQ** probe complex structures obtained from docking were used as input configurations for MD. The **CQ** molecular structure as in docked state is constrained and only the added hydrogen atoms positions were optimized at B3LYP/6-311++G(d,p) level of theory using Gaussian09 software (Singh et al., 1984). The charges for **CQ** probe were obtained from best fitting to molecular electrostatic potential using the CHELPG procedure, as implemented in Gaussian09 software. These charges of **CQ** probe were, used in the subsequent molecular dynamics and free energy simulations. The Aβ42 fibril:**CQ** probe complex is solvated with approximately 15000 water molecules in an orthorhombic simulation box. Single chloride was added to neutralize the probe molecule and sufficient number of sodium ions were added to neutralize the entire fibril:probe complex systems. In order to describe non-bonded interactions of various subsystems namely **CQ** probe, amyloid fibril and water, the force-fields namely GAFF, ff99SB, and TIP3P were used respectively. The calculations were carried out in isothermal-isobaric ensemble using amber/12 software (Wang et al., 2004; Jorgensen et al., 1983; Case et al., 2012). The time step for the integration of equation of motion was kept to be 2 fs and the total time scale for the production run was approximately around 10 ns. During the initial MD simulation, the backbone carbon atoms of pentamer units were constrained with weak harmonic potential (with force constant value 1 kcal/mol/Å^2). For the production run, whole fibril was modeled using fully flexible model without any constraint. The trajectories corresponding to last 4 ns were used for the free energy calculations using MM/GBSA approach. This includes van der Waals, electrostatic, polar and non-polar solvation energies and entropic (obtained using normal modes calculations) as contributions to total free energy. The free energy difference between the complex and sum of individual subsystems provides the estimate for the binding free energy. The binding affinity for **CQ** probe in the four binding sites are displayed in

Table S1 which shows that in all sites **CQ** has larger binding affinity to fibril in comparison to ThT. This explains the experimentally observed result wherein **CQ** replace ThT bound to fibril.

Table S1. The binding free energy for **CQ** in different binding sites of Aβ42 fibril (dodecamer)

System	**E_{vdw}**	**E_{elec}**	**E_{polar}**	**$E_{nonpolar}$**	**Entropy**	**BE, kcal/mol**
Site 1	-59.8	112.1	-97.7	-4.8	22.8	-27.4
Site 2	-48.8	-168.7	186.3	-4.0	14.5	-20.7
Site 3	-40.3	162.0	-145.5	-3.7	20.5	-7.0
Site 4	-58.1	145.4	-134.4	-4.1	23.7	-27.5

Our experimental data showed specific and selective interaction of **CQ** probe with Aβ42 fibril, while no significant binding to fibrils of IAPP and α-Syn observed. In order to understand the binding affinity of **CQ** probe towards amyloid beta fibrils, the above protocol was used. The negligible binding of **CQ** probe to fibrils of IAPP and α-Syn has been addressed by estimating the binding affinity of the probe with these fibril structures. The methodologies to set up input structures to perform MD and to calculate the binding free energies are the same as above. The structure reported in reference and structure with reference number 2n0a reported in protein data bank were used for IAPP and for α-Syn, respectively (Luca et al., 2007; Tuttle et al., 2016). The detailed procedure involved the molecular docking, molecular dynamics followed by free energy calculations using MM-GBSA approach. Various binding sites for IAPP and α-Syn targets are shown in Fig. S10. Both fibril structures are shown to have surface and core binding sites for **CQ** probe similar

to Aβ42 fibril. The binding affinities of **CQ** probe in different binding sites of these fibrils are displayed in Table S2 and S3. As can be seen, the binding affinities of **CQ** towards IAPP and α-Syn in all sites are many order smaller when compared to the Aβ42 fibril, which explains why **CQ** probe binds strongly with the latter target.

Table S2. The binding free energy for **CQ** in different binding sites of IAPP fibril (pentamer)

Site	**E_{vdw}**	**E_{elec}**	**E_{polar}**	**$E_{nonpolar}$**	**Entropy**	**BE, kcal/mol**
Site 1	-36.2	164.8	-148.6	-2.5	18.8	-3.7
Site 2	-48.7	314.0	-283.1	-4.0	19.9	-1.9
Site 3	-37.9	430.3	-407.6	-3.0	21.1	2.9
Site 4	-41.7	344.1	-321.3	-3.7	18.9	-3.7

Table S3. The binding free energy for CQ in different binding sites of α-syn fibril (dodecamer)

Site	**E_{vdw}**	**E_{elec}**	**E_{polar}**	**$E_{nonpolar}$**	**Entropy**	**BE, kcal/mol**
Site 1	-33.8	41.8	-26.4	-3.3	19.0	-2.7
Site 2	-52.9	3.9	36.3	-4.6	21.0	3.7
Site 3	-33.0	232.1	-213.7	-2.6	20.0	2.8
Site 4	-52.3	74.9	-38.9	-3.9	19.4	-0.8

1.10 Static and dynamic electronic structure calculations. In order to study the fibril specific optical properties of the **CQ** probe, two sets of time dependent density functional

theory calculations were carried out namely TD-DFT/PCM and TD-DFT/MM (Olsen et al., 2010). In particular, the latter approach explicitly treats the solvent and fibril environment, and the **CQ** and environmental interactions are accounted through electrostatic embedding scheme. The former does not account for configurational averaging and employs a polarizable continuum model for the solvent description. The latter one is carried out for various configurations obtained from QM/MM MD simulations and account for temperature effect and the properties are obtained as configurational average. We describe the computational details for both approaches below. The molecular geometry of **CQ** has been optimized in two solvents namely chloroform and water using density functional theory at the level of B3LYP/6-311++G**. The solvent description is based on polarizable continuum model as implemented in Gaussian09. The absorption spectra of **CQ** has been computed as vertical excitation energy using the optimized ground state geometries. In particular, the TD-DFT/PCM calculations for **CQ** in chloroform and water solvents were carried out on the optimized geometries in respective solvents. The size of the cavity for the solute is based on the default values in the PCM implementation in gaussian09 software. These calculations were carried out to provide first-hand information about the origin for the fibril-induced red shift in the absorption spectra of **CQ** (since chloroform solvent partly mimics the hydrophobic microenvironment as in fibril). The second set of calculations employs the TD-DFT/MM approach where the **CQ** probe is described using density functional level of theory at B3LYP/Turbomole-TZVP basis set while the fibril and solvent environments are described using a force-field which is the same as the one used in MD. Since there are no polarizable force-fields available for fibril, we used charges-only-force-field for the environment (for both fibril and solvents). The calculations were carried out by including the whole fibril and water molecules within 15 Å from the probe center of mass. A representative snapshot configuration is shown in Fig. S11. For each fibril:**CQ** probe complexes such TD-DFT/MM

calculations were carried out and the final one photon absorption spectra was computed as average over 50 configurations. The spectral calculations were obtained by convoluting the six lowest energy excitations. The absorption spectra for **CQ** in water was computed using combined MD+ TD-DFT/MM approach similar to the one as explained above. It has been observed that the absorption spectra of **CQ** in all binding sites of fibril are red shifted when compared to in water solvent (the results are not shown). However, the computed red shift is over estimated in some of the sites, which may be because we employed non-polarizable force-field for fibril and solvent.

1.11 BBB permeability. BBB permeability of the probe **CQ** was assessed by injecting **CQ** (250 μL of 1 mg/mL of **CQ** dissolved in PBS buffer) intraperitoneally into 6 weeks old BALB C mice (4 mice). As control PBS solution (2 mice) was injected into the mice. After one hour the mice were sacrificed and the mice brains were carefully extracted from the skull. Each mice brain was thoroughly washed with PBS and transferred into 3 mL of RIPA buffer. The brain was mechanically homogenized for 10 min, and the solution was transferred to falcon tubes followed by centrifugation at 4000 rpm at 4 °C. The supernatants of each sample was passed through 0.2 micron filter and absorption of the brain lysate was measured at 516 nm (absorption maxima of **CQ**) to determine the BBB permeability of **CQ** into the brain.

References

Case, D. A., Darden, T. A., Cheatham, T. E. III, Simmerling, C. L., Wang, J., Duke, R. E., Luo, R., Walker, R. C., Zhang, W., Merz, K. M., et al. 2012, Amber 12; University of California: San Francisco

Frisch, M. J., Trucks, G. W., Schlegel, H. B., Scuseria, G. E., Robb, M. A., Cheeseman, J. R., Scalmani, G., Barone, V., Mennucci, B., Peterssen, G. A., et al. 2010, Gaussian 09, Revision C.01; Gaussian, Inc.: Wallingford, CT.

Jorgensen, W. L., Chandrasekhar, J., Madura, J. D., Impey, R. W., Klein, M. L., 1983, J. Chem. Phys. 79, 926–935.

Lesne, S., Teng Koh, M., Kotilinek, L., Kayed, R., Glabe, C. G., Yang, A., Gallagher, M., Ashe, K. H., 2006, Nature 440, 352−357.

Luca, S., Yau, W. M., Leapman, R., Tycko, R., 2007, Biochemistry 46, 13505−13522.

Lührs, T., Ritter, C., Adrian, M., Riek-Loher, D., Bohrmann, B., Döbeli, H., Schubert, D., Riek, R., 2005, Proc. Natl. Acad. Sci. U. S. A. 102, 17342–17347.

Maity, D., Govindaraju, T., 2010, Inorg. Chem. 49 , 7229 –7231.

Miller III, B. R., McGee Jr, T. D., Swails, J. M., Homeyer, N., Gohlke, H., Roitberg, A. E., 2012, J. Chem. Theory Comput. 8, 3314–3321.

Morris, G. M., Huey, R., Lindstrom, W., Sanner, M. F., Belew, R. K., Goodsell, D. S., Olson, A. J., 2009, J. Comput. Chem. 16, 2785–91.

Olsen, J. M., Aidas, K., Kongsted, J., 2010, J. Chem. Theory Comput. 6, 3721−3734.

Singh, U. C., Kollman P. A., 1984, J. Comput. Chem. 5, 129–145.

Tuttle, M. D., Comellas, G., Nieuwkoop, A. J., Covell, D. J., Berthold, D. A., Kloepper, K. D., Courtney, J. M., Kim, J. K., Barclay, A. M., Kendall, A., Wan, W., Stubbs, G., Schwieters, C. D., Lee, V. M. Y., George, J. M., Rienstra, C. M., 2016, Nat. Struct. Mol. Biol. 23, 409–415.

Wang, J., Wolf, R. M., Caldwell, J. W., Kollman, P. A., Case, D. A., 2004, J. Comput. Chem., 25, 1157−1174.

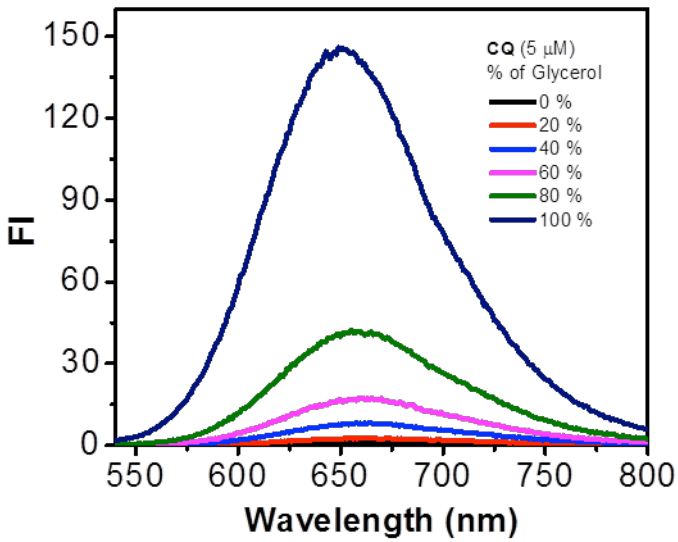

Fig. S1. A) Fluorescence intensity (FI) of **CQ** (5 mM, 10 mM PBS) with increasing percentage of glycerol (20%, 40%, 60%, 80% & 100%).

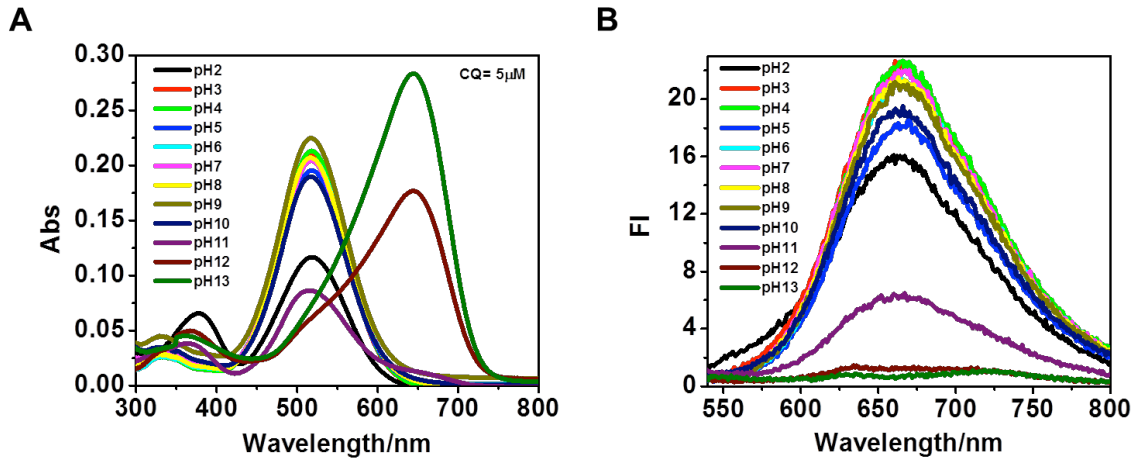

Fig. S2. Absorption (A) and emission (B) spectra of probe **CQ** at different solution pH.

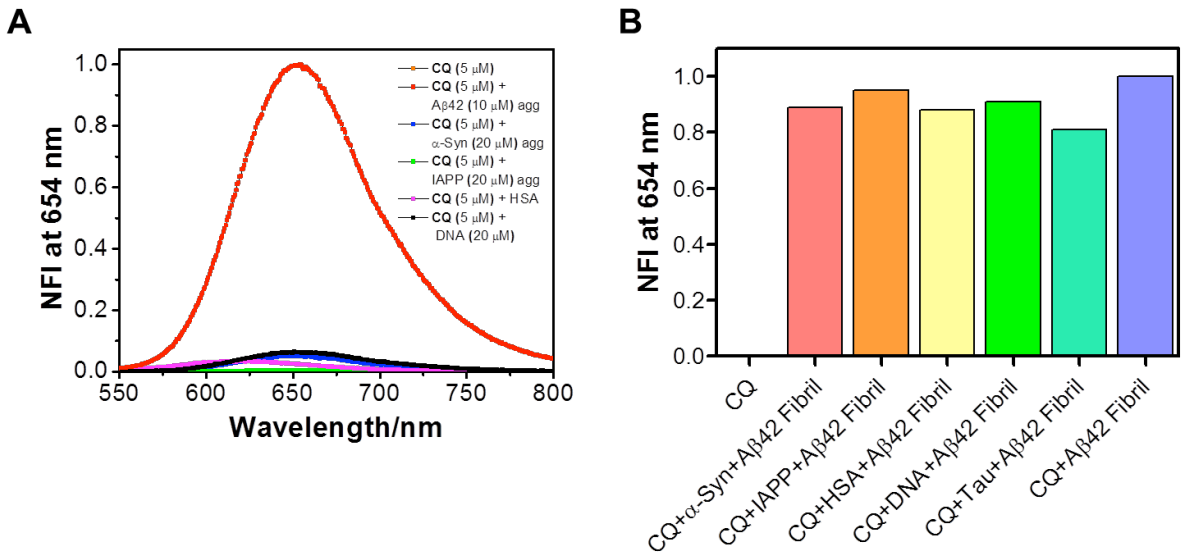

Fig. S3. A) Normalized fluorescence intensity (NFI) of **CQ** in presence of α-Syn aggregates (20 mM), IAPP aggregates (20 mM), HSA (20 mM) and calf thymus DNA (20 mM). B) NFI of **CQ** in presence Aβ42 fibrillar aggregates (10 μM) containing α-Syn aggregates (20 μM), IAPP aggregates (20 μM), DNA (20 μM), HSA (20 μM) or tau aggregates (20 μM).

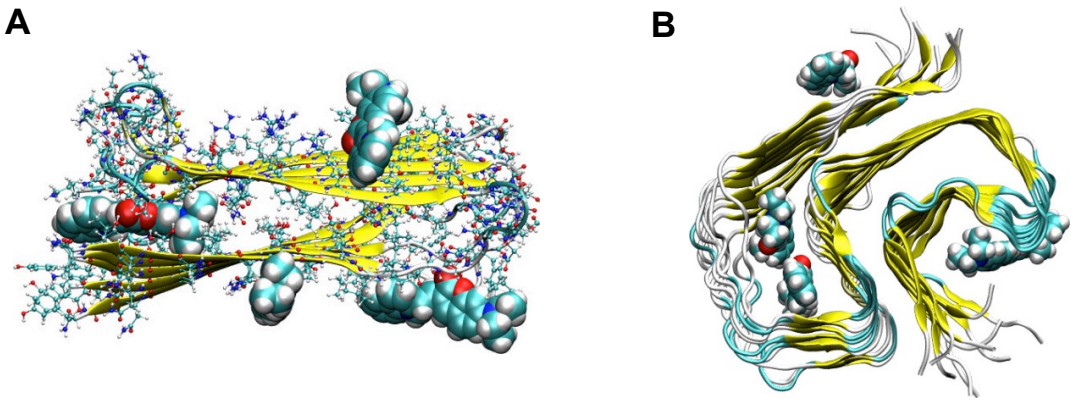

Fig. S4. Various binding sites for **CQ** in protofibrils of IAPP and α-Syn.

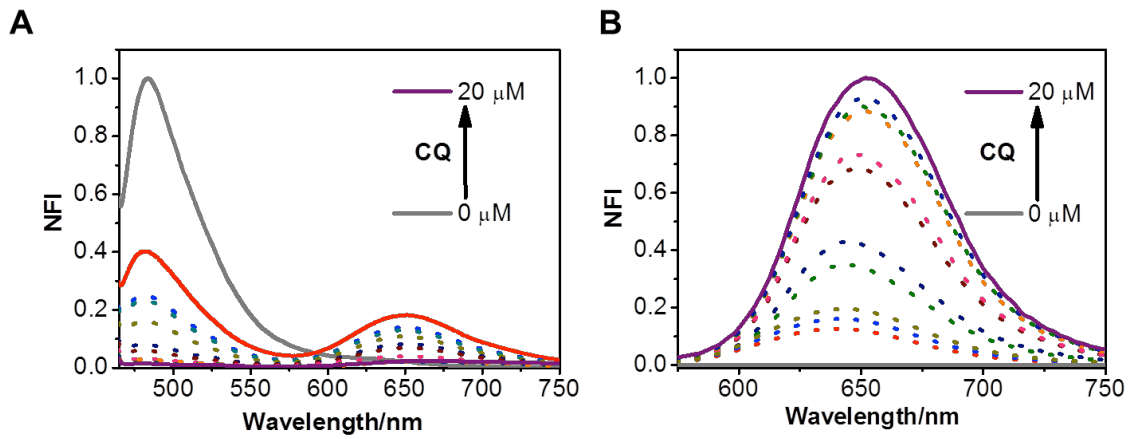

Fig. S5. FRET and displacement assay. A) Fluorescence intensities of ThT and **CQ** (λ_{ex} at 450 nm; fluorescence at 485 nm and ~654 nm) upon titration of a ThT/Aβ42 fibrillar aggregates complex (ThT, 10 mM/Aβ42 fibrillar aggregates, 20 mM) with **CQ**. B) Fluorescence intensities of **CQ** (λ_{ex} at 521 nm; fluorescence measured at ~654 nm) upon titration of a ThT/Aβ42 fibrillar aggregates complex with **CQ**.

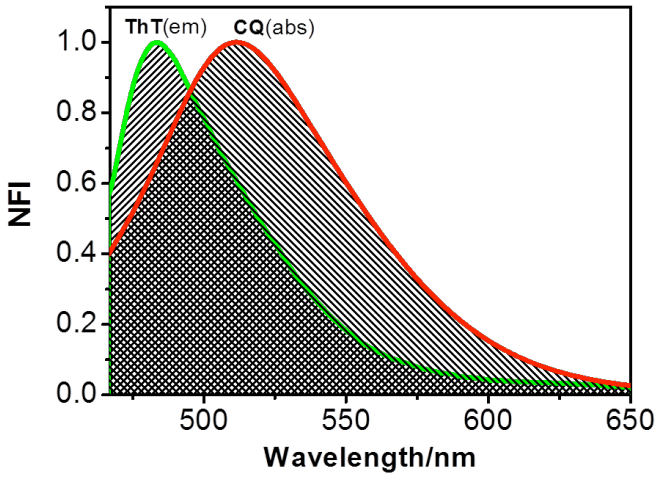

Fig. S6. Spectral overlap for the emission of ThT and absorption of **CQ,** showing favourable condition for FRET from ThT to **CQ**.

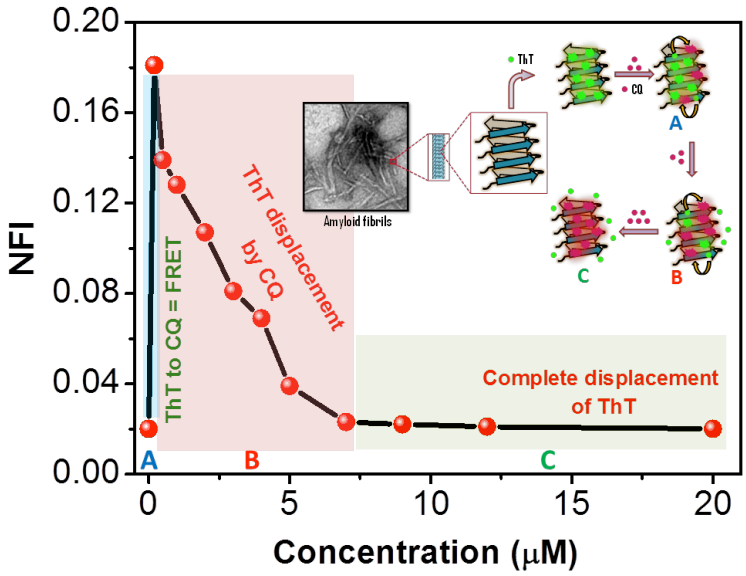

Fig. S7. FRET and displacement assay. The fluorescence intensity of **CQ** (λ_{ex} at 450 nm; fluorescence measured at ~654 nm) upon titration of a ThT/Aβ42 fibrillar aggregates complex with **CQ**. Inset: Proposed model for the FRET and displacement studies of **CQ** with ThT/Aβ42 fibrillar aggregates complex.

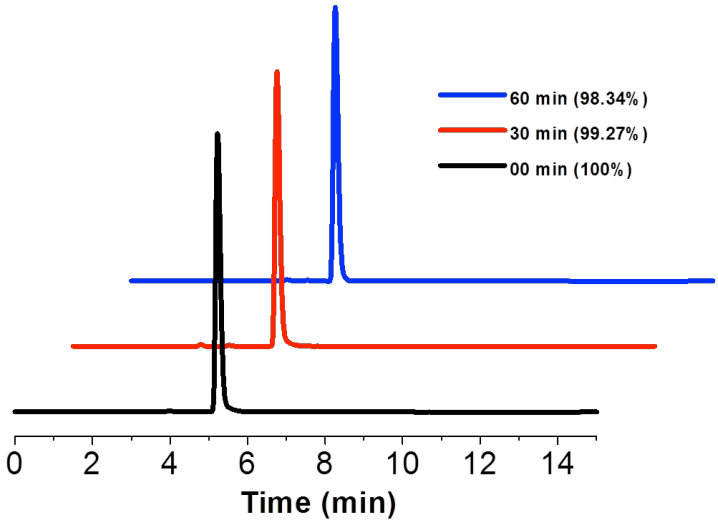

Fig. S8. *In vitro* stability assay. **CQ** exhibit high *in vitro* stability in HBS and > 97% of the probe was identified intact through LCMS after 60 min of incubation with HBS at 37 °C.

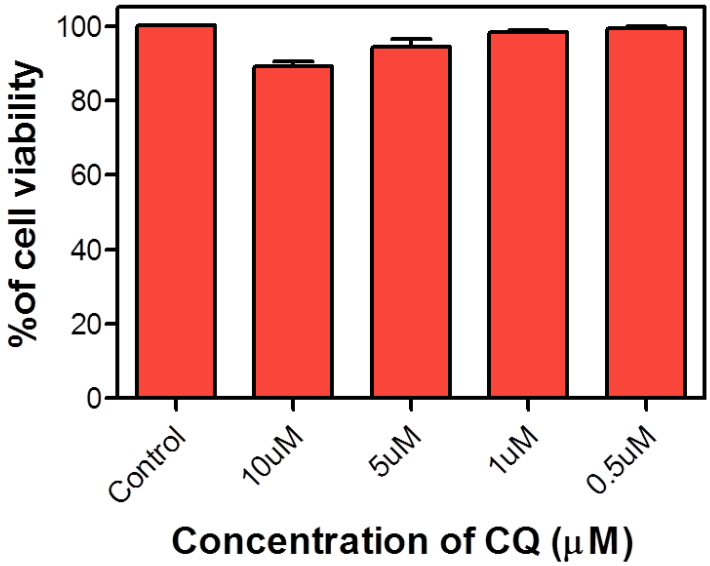

Fig. S9. Cell viability assay (MTT assay) of probe **CQ** with varying concentrations in PC12 cells.

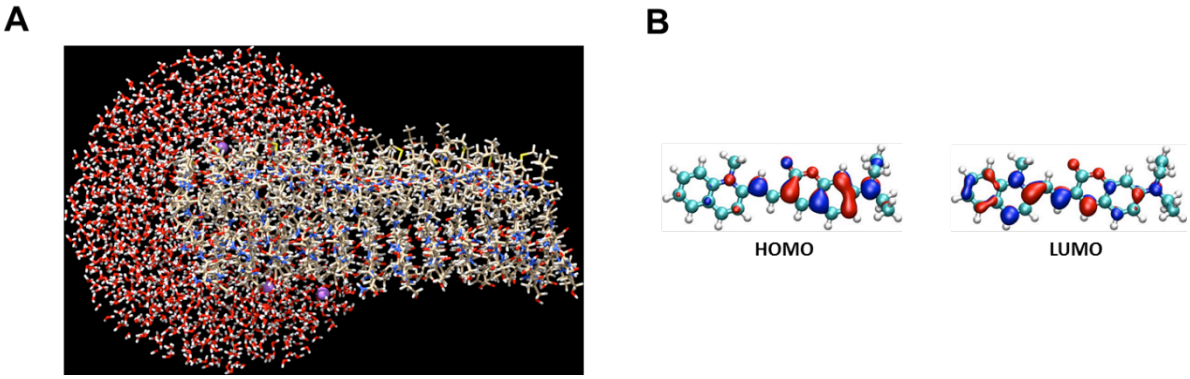

Fig. S10. A) Snapshot configuration for fibril:**CQ** (in site-1) complex in water used for TD-DFT/MM calculation. The water solvents and ions within 15 Å from the center of mass of **CQ** probe are included explicitly in the calculation. **B**) HOMO and LUMO Molecular orbitals involved in the low energy excitation.

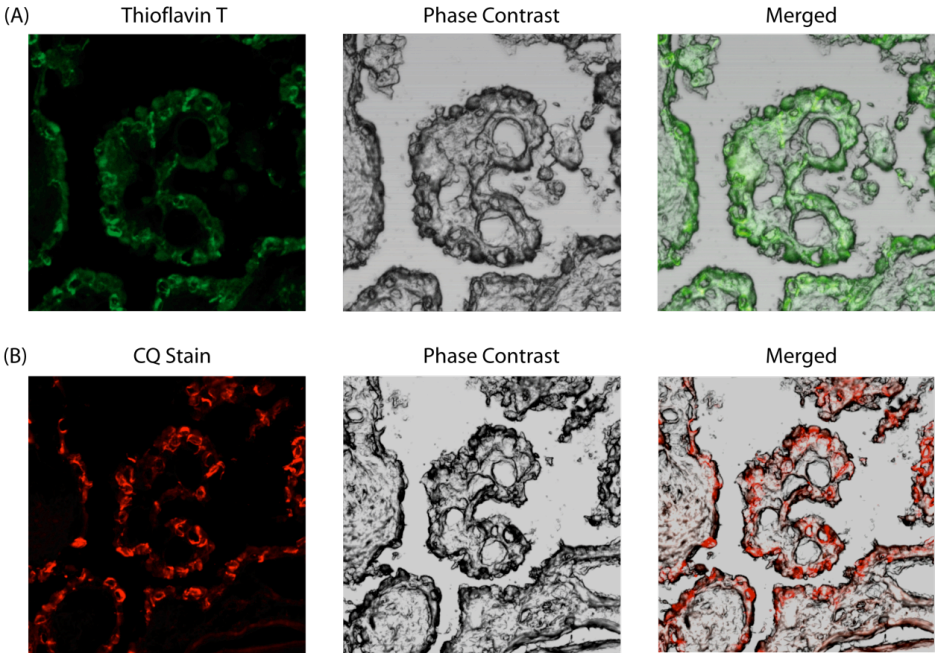

Fig. S11. CQ reveals the structure and localization of amyloid angiopathy. High resolution imaging of identical human brain cross sections independently stained using **CQ** or ThT. (A) ThT stains amyloid angiopathy but produces increased background fluorescence, which impedes the visualization of the ring shaped aggregates along the outer wall of the tissue. (B) **CQ** specifically stains the amyloid angiopathy and reveals ring-shaped aggregates accumulated along the outer wall of the tissue.

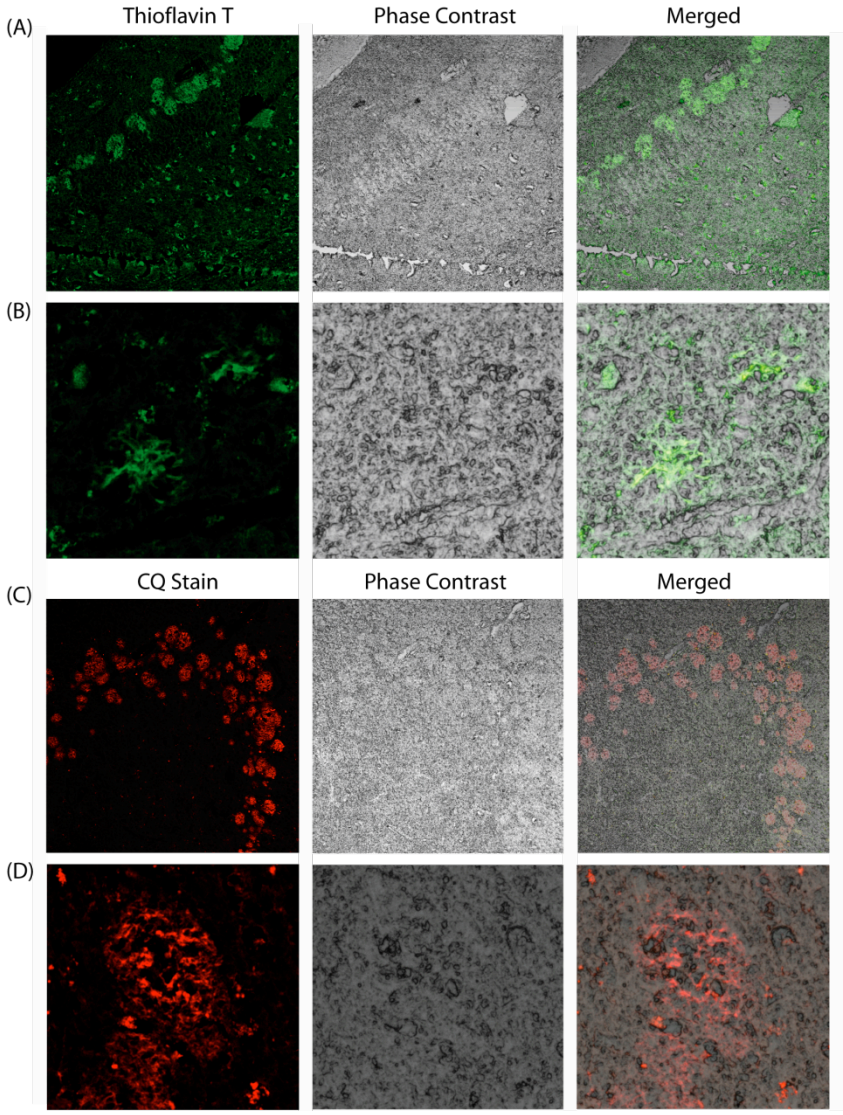

Fig. S12. CQ stains multiple forms of amyloid plaques with high selectivity**.** Comparative staining of different amyloid plaques by **CQ** and ThT (A) ThT stains for amyloid plaques and neurofibrillary tangles. (B) High-resolution image of a core plaque visualized using ThT. (C) **CQ** stains amyloid plaques but not neurofibrillary tangles. (D) High-resolution of a diffused plaque visualized using **CQ**. The high signal-to-noise ratio allows for visualization of the structural features of the aggregates.

^{1}H NMR of **CQ** (DMSO-d_6)

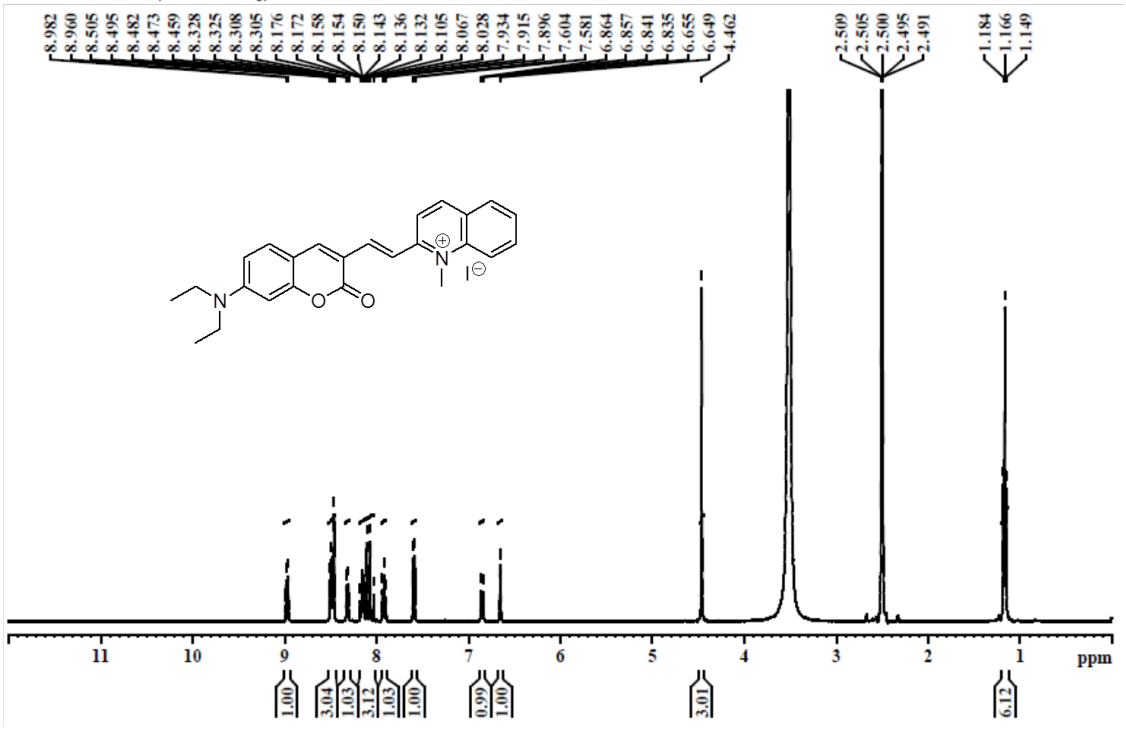

^{13}C NMR of **CQ** (DMSO-d_6)